The published version of this manuscript appeared in *IEEE Transactions on Applied Superconductivity* **19**, No. 3, Part 3, 3455 - 3458 (2009)

Growth Conditions of Sequentially Electrodeposited Buffer Layers for YBCO Superconductor

Sovannary Phok, Wenjun Zhao, and Raghu Bhattacharya

***Abstract*— We report recent technical advances in the fabrication by sequential electrodeposition (ED) of buffer architectures with two stacking layers. The proposed approach is to fabricate a structure containing a pyrochlore oxide and Gd_2O_3, which takes advantage of the low oxygen diffusivity in pyrochlores and the excellent crystal lattice match of Gd_2O_3 and $YBa_2Cu_3O_{7-\delta}$ (YBCO). A systematic study is performed for a fundamental understanding of the buffer structure grown by ED. The electrolyte composition, solution flow rate, composition/concentration of chemicals, and annealing conditions are found to affect considerably the deposition of the layer, formation of the pyrochlore oxide, and film texture.**

***Index Terms*— Buffer layers, Electrodeposition, Pyrochlore compound, RE_2O_3 compound, Texture.**

I. INTRODUCTION

FOR several decades, intensive research and development efforts have been carried out to integrate superconductor films into various devices such as cables, transformers, current limiters, magnets, and motors. YBCO films prepared on rolling-assisted biaxially textured substrates (RABiTS) [1] and also YBCO films prepared by ion-beam assisted deposition (IBAD) [2] on non-textured substrates have shown promising performance with MA/cm^2 current density at 77 K [3]. The RABiTS process is based on the deposition of an epitaxial oxide buffer layer on a textured metal substrate. The buffer layer structure, a stack of at least three oxide layers, functions as a template for the growth of the YBCO superconducting layer and prevents metal and oxygen diffusions between the substrate and the superconductor.

To produce coated conductors in lengths of 100 meters or more, some important issues (such as slow production rate, high cost, and inhomogeneity in long tapes) need to be resolved in these thin-film technologies [4]. Our approach to the fabrication of coated conductors is based on non-vacuum techniques; in particular, electrodeposition has potential [5] for fabricating long-length, high-rate, low-cost tapes.

Among the materials compatible with YBCO, oxides with structures of perovskite ($LaMnO_3$), fluorite (CeO_2), pyrochlore ($Gd_2Zr_2O_7$), and REO (Gd_2O_3) have shown promising properties as oxygen barriers. We have focused our efforts on two simplified buffer architectures: $Gd_2O_3/Gd_2Zr_2O_7$ and $CeO_2/Gd_2Zr_2O_7$ on a RABiTS Ni-W substrate, which takes advantage of the low oxygen diffusivity in pyrochlores and the excellent crystal lattice match of CeO_2 and Gd_2O_3 with YBCO. The processing steps are as follows:

1. Electrodeposition of $Gd_2Zr_2O_7$ layer on Ni-W substrate
2. Electrodeposition of Gd_2O_3 or CeO_2 on $Gd_2Zr_2O_7$ layer
3. Single ex-situ thermal treatment.

Buffer layers with optimal physical properties and morphology are indispensable for the growth of highly superconducting thin film. Texture and surface morphology in particular are crucial for the application of the films in planar multilayer devices such as coated conductors. We obtained very high-quality electrodeposited buffer layers by optimizing the electrolyte composition at a fixed deposition current density and also optimizing the subsequent thermal treatments. In this paper, we report on the effect of the electrolyte mixture and the thermal treatments on the formation of electrodeposited $Gd_2Zr_2O_7$ and $Gd_2O_3/Gd_2Zr_2O_7$ layers.

II. EXPERIMENTAL DETAILS

$Gd_2Zr_2O_7$ films were electrodeposited from a bath containing 5 mM of gadolinium bromide and 2 mM of zirconium bromide dissolved in dimethyl sulfoxide (DMSO) and ethanol solution mixture. Electrodeposition was performed at an optimal current density of 1 mA/cm^2 and under constant stirring in a vertical two-electrode cell configuration. The average rate of deposition was about 30 nm/min. Gd_2O_3 films were electrodeposited using an aqueous bath under constant stirring and containing 6 mM of gadolinium bromide. The average rate of deposition was about 5 nm/min.

Composition and thickness of electrodeposited films were obtained from inductively coupled plasma (ICP) analysis. The annealed films were characterized by X-ray diffraction (XRD) using copper Kα radiation (λ = 1.56054 Å). Phase identification was performed in Bragg Bretano geometry (θ/2θ geometry). The mosaic spread of $Gd_2Zr_2O_7$ grains along the *c*-

Manuscript received 19 August 2008.

This work has been performed by an employee of the Midwest Research Institute under Contract No. DE-AC36-99GO10337 with the U.S. Department of Energy. The United States Government retains a non-exclusive, paid-up, irrevocable, worldwide license to publish or reproduce the published form of this work.

S. Phok, W. Zhao, and R. Bhattacharya are with the National Renewable Energy Laboratory, Golden, CO 80401 USA (phone: 303-384-6413; fax: 303-384-6432; e-mail: sovannary_phok@nrel.gov).

axis and in-plane texture were determined by rocking curve scans on the (004) reflection [2θ=33.90 (±0.15)º] and pole figure scans on the (222) reflection [2θ=29.30 (±0.03)º], respectively. The mosaic spread of Gd_2O_3 grains along the *c*-axis and in-plane texture were determined by rocking curve scans on the (002) reflection [2θ= 32.93 (±0.03)º] and pole figure scans on the (111) reflection [2θ= 28.45 (±0.03)º], respectively. The angular dispersion of $Gd_2Zr_2O_7$ and Gd_2O_3 grains in (*a*,*b*) plane was calculated from the peak broadening of φ-scans on the (222) reflection [$Gd_2Zr_2O_7$: 2θ=29.30 (±0.03)º and χ=54.7º] and (111) reflections [Gd_2O_3: 2θ= 28.45 (±0.03)º], respectively. Morphology and roughness of films were revealed from scanning electron microscopy (SEM) scans and optical profiler scans.

III. RESULTS AND DISCUSSION

A. Effect of the electrolyte mixture on the electrodeposited $Gd_2Zr_2O_7$ layers

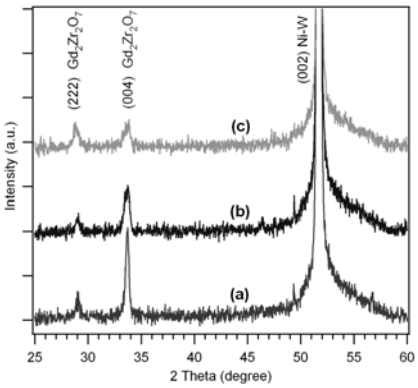

Fig. 1. X-ray diffraction after annealing at 950 °C of $Gd_2Zr_2O_7$ layers electrodeposited from electrolytes containing: (a) 6% ethanol, (b) 10% ethanol, and (c) 13% ethanol.

In this set of experiments, concentration of Gd^{3+} and Zr^{3+} ions were set to 5 and 2 mM, respectively. The films were deposited at a rate of 700 rpm with constant stirring by a magnetic stirring bar. We maintained a constant stirring speed to prevent inhomogeneities in the deposited films. Various electrolytes were selected for the deposition of $Gd_2Zr_2O_7$ layer on Ni-W substrate. The challenge in the electrodeposition of $Gd_2Zr_2O_7$ is to obtain crack-free and smooth surface morphology. A smooth and crack-free gadolinium oxide layer was easily electrodeposited from an aqueous media. On the other hand, the surface morphology of the zirconia layer electrodeposited from $ZrOCl_2.xH_2O$ in aqueous media was poor. The layer deposited from a stagnant aqueous solution was reported to yield a rough surface with cracks [6,7]. Zirconia layers deposited from an organic solvent, DMSO, and alcohol were crack-free [8,9]. Thus a mixture of DMSO and ethanol was selected to electrodeposit the $Gd_2Zr_2O_7$ layer. The depositions were performed from various electrolytes containing 6%, 10%, and 13% ethanol in DMSO. Compositions of the electrodeposited layers were approximately Ga:Zr=1.27:0.73, Ga:Zr=1.28:0.72, and Ga:Zr=1.32:0.68, respectively. The thickness of the deposited layers was 75, 70, and 63 nm, respectively, when deposited using a 3-min deposition time for all films. ICP analysis revealed an increase of gadolinium in the layer and decreasing layer thickness when ethanol concentration was increased in the electrolyte. We also note that for electrolytes with high ethanol concentrations (>13%), a faster flow rate was necessary to prevent the formation of rough surface; this is probably due to the deposition of a gel-like layer containing saturated hydrocarbon, as has been observed in previous work [9]. As-deposited layers were amorphous, smooth, and crack free, as observed by an optical profiler. The layers were subsequently annealed at 950 °C for 1 to 5 h in an Ar:H_2 gas mixture. The optimization of the gas mixture has been reported previously for the fabrication of textured ceria layers electrodeposited on Ni-W substrate [10]. A mixture of Ar:0.5%H_2 was selected for all processing temperatures, based on previous work.

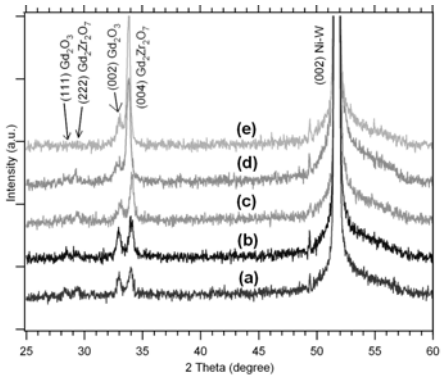

Fig. 2. X-ray diffraction of electrodeposited $Gd_2O_3/Gd_2Zr_2O_7$ on Ni-W substrate after annealing in Ar: H_2 gas flow at 1100 °C for (a) 1, (b) 2, (c) 3, (d) 4, and (e) 5 h.

XRD patterns of the three electrodeposited layers are shown in Figure 1. Patterns (a), (b), and (c) correspond to the layers electrodeposited in 6%, 10%, and 13% ethanol, respectively. Figure 1 shows three diffraction peaks at $2\theta = 28.83$ (±0.16)°, 33.66 (±0.05)°, and 51.6 (±0.03)°. The two peaks at 28.83° and 33.66° were identified as $Gd_2Zr_2O_7$ (222) and (004) reflections, respectively. The peak at 51.6 (±0.03)° is a Ni-W (002) reflection. In addition, Figure 1 shows a decreasing relative intensity of the $Gd_2Zr_2O_7$ (004) reflection in (b) and (c). As diffraction intensity is related to the crystallinity of the layer, the results suggest a decrease in crystallinity and grain growth for the layers electrodeposited in 10% and 13% ethanol. The increase of gadolinium content in the layer probably induces an amorphization of the layer. The best crystalline layer was obtained using 6% ethanol. However, misorientation along <111> axis was detected. The presence of (222) reflection is probably related to the non-stoichiometry of the layer as well as to the non-optimized annealing conditions. We optimized the annealing condition of the films obtained from 6% ethanol solution to eliminate the misorientation.

B. Ex-situ growth conditions for textured buffer stacking

Complete electrodeposited buffer architecture of the type $Gd_2Zr_2O_7/Gd_2O_3$ was deposited. About 60–70-nm-thick $Gd_2Zr_2O_7$ layers were deposited from a bath containing 6%

ethanol. A Gd_2O_3 cap layer about 30 nm thick was electrodeposited from an aqueous bath. The buffer layers were annealed at 1100 °C in H_2:Ar gas for 1 to 5 h. XRD patterns of the five samples are shown in Figure 2. Pattern (a), (b), (c), (d), and (e) are from the layers annealed for 1, 2, 3, 4, and 5 h, respectively. Three distinctive diffraction peaks at 2θ = 33.00 (± 0.05)°, 34.01 (± 0.05)°, and 51.60 (± 0.03)° were identified as Gd_2O_3 (002), $Gd_2Zr_2O_7$ (004), and Ni-W (002) reflections, respectively. We observed an increase in relative intensity for the $Gd_2Zr_2O_7$ reflection when annealed for a longer time. As shown in Figure 2, the $Gd_2Zr_2O_7$ (004) reflection became four times more intense on annealing for 5 h compared to 1 h. As expected, an improvement of crystallinity, and therefore an improvement of grain growth, was obtained when the annealing time increased. Thus, a long annealing time of 4 to 5 h seemed to favor the grain growth in the $Gd_2Zr_2O_7$ layer. The relative intensity of the Gd_2O_3 (002) reflection remained similar in the five XRD patterns of Figure 2. No significant improvement in the crystallinity of GO layers was detected by XRD. One possible cause could be the limitation of the XRD technique for measuring such very thin layers.

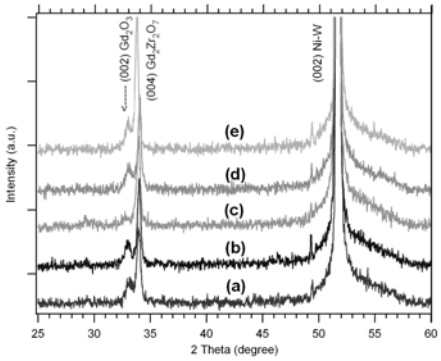

Fig. 3. XRD of electrodeposited $Gd_2O_3/Gd_2Zr_2O_7$ on Ni-W substrate after annealing in Ar:H_2 gas flow at (a) 800, (b) 950, (c) 1000, (d) 1050, and 1100 °C for 5 h.

Following the optimization of annealing time, we optimized the annealing temperature. The buffer layers were annealed at temperatures ranging from 800 to 1100 °C. Figure 3 shows the XRD patterns of Gd_2O_3/ $Gd_2Zr_2O_7$ layers annealed for 5 h in Ar:H_2 gas at temperatures of (a) 800, (b) 950, (c) 1000, (d) 1050), and (e) 1100 °C, respectively. A significant variation in intensity was detected on the $Gd_2Zr_2O_7$ (004) reflection. We noted an increase of relative intensity, and thus an improvement in crystallinity and grain growth, when the temperature was increased from 800 to 1100 °C. No misorientation was detected by XRD, even for temperatures as low as 800 °C. $Gd_2O_3/Gd_2Zr_2O_7$ layers with the best crystallinity were obtained from a 5-h annealing at 1100 °C.

C. Electrodeposited $Gd_2O_3/Gd_2Zr_2O_7$ bilayer on Ni-W substrate

Gd_2O_3 cap layers were electrodeposited on $Gd_2Zr_2O_7$ layers from 10 to 60 nm thick to determine the optimum cap layer thickness for YBCO growth. Surface morphology and texturing of $Gd_2O_3/Gd_2Zr_2O_7$ bilayers were analyzed for samples annealed at 1100 °C for 5 h. XRD patterns of the $Gd_2O_3/Gd_2Zr_2O_7$ layers are shown in Figure 4; (a), (b), (c), and (d) are from the Gd_2O_3 buffer layers of 10, 20, 30, and 60 nm thicknesses, respectively. Patterns (a) and (b) show a distinctive reflection at 2θ = 33.98 (± 0.09)°, identified as a $Gd_2Zr_2O_7$ (004) reflection. Patterns (c) and (d) show an additional XRD peak at 2θ = 32.93 (± 0.03)°, which we identified as a Gd_2O_3 (002) reflection. No misorientation was observed in the patterns. The grains in both Gd_2O_3 and $Gd_2Zr_2O_7$ layers were aligned along the c-axis, as shown by the presence of (00*l*) reflections only. In addition, analysis of the 2θ peak position revealed a shift of the $Gd_2Zr_2O_7$ (004) reflection toward low angles, suggesting an increase of the d-spacing of $Gd_2Zr_2O_7$ when the thickness of Gd_2O_3 increased.

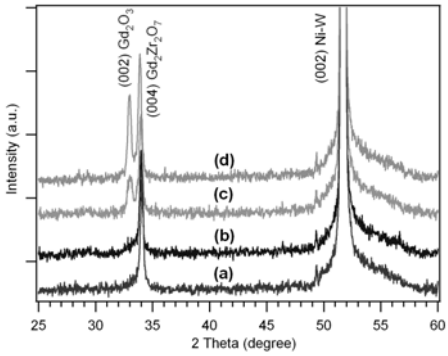

Fig. 4. X-ray diffraction of electrodeposited $Gd_2O_3/Gd_2Zr_2O_7$ on Ni-W substrate with various thicknesses of the GO layer: (a) 10, (b) 20, (c) 30, and (d) 60 nm after annealing in H_2:Ar gas flow at 1100 °C for 5 h.

Surface morphologies of these films were analyzed by SEM. Micrographs (a) and (b) in Figure 5 show the surface of the annealed $Gd_2Zr_2O_7$ layer and $Gd_2O_3/Gd_2Zr_2O_7$ bilayer with a 30-nm-thick Gd_2O_3 cap layer, respectively. Both micrographs revealed smooth and crack-free surfaces with roughness of about 3 nm [5]. The $Gd_2Zr_2O_7$ layer shown in Figure 5(a) has more defects compared to the $Gd_2O_3/Gd_2Zr_2O_7$ layer in Figure 5(b). These defects are due primarily to the voids in the films, confirmed by TEM study of $Gd_2Zr_2O_7$ and $Gd_2O_3/Gd_2Zr_2O_7$ [11]. The electrodeposited $Gd_2Zr_2O_7$ layer had a void density as high as 10^{16} cm^{-2}. On the other hand, a TEM of the $Gd_2O_3/Gd_2Zr_2O_7$ stacking revealed a dense, crystalline, and textured Gd_2O_3 cap layer without any voids, which is ideal for the growth of good-quality YBCO films.

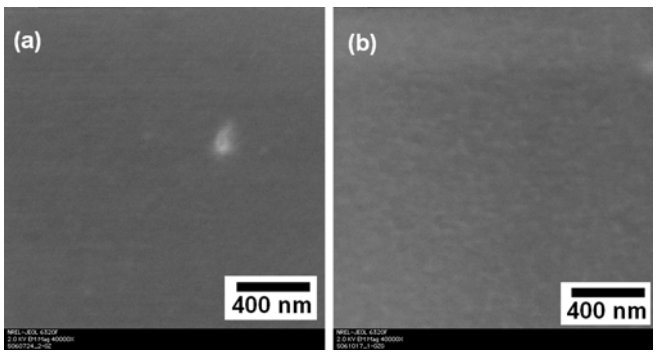

Fig. 5. Scanning electron micrographs of (a) annealed GZO layer and (b) GO/GZO layer with a 30-nm-thick GO cap on Ni-W substrate.

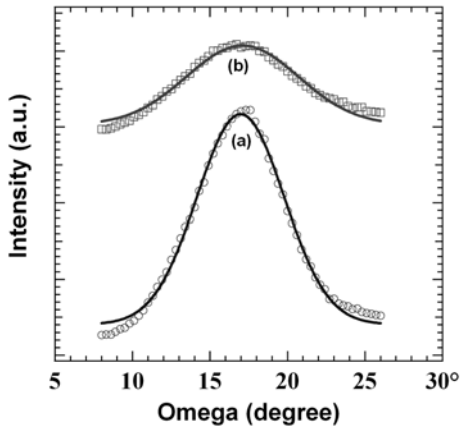

Fig. 6. Out-of-plane alignment of GO and GZO grains in electrodeposited GO/GZO layers annealed at 1100 °C for 5 h; omega scans of (a) GZO (004) reflection at 2θ= 33.95° and (b) GO (002) reflection at 2θ=32.93°.

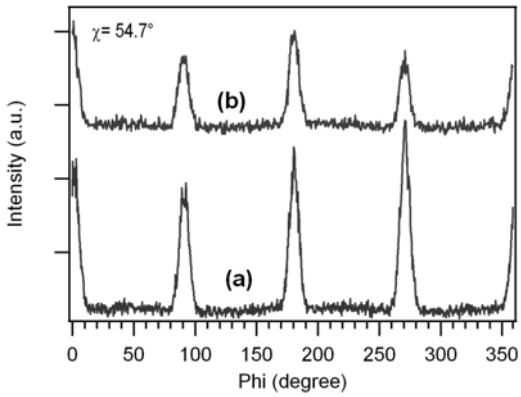

Fig.7. In-plane alignment of GO and GZO grains in a GO/GZO buffer structure annealed at 1100 °C for 5 h; phi scans of (a) GZO (222) reflection 2θ = 29.30° and (b) GO (111) reflection at 2θ=28.45°.

Out-of-plane and in-plane alignments of $Gd_2Zr_2O_7$ and Gd_2O_3 grains are shown in Figures 6 and 7, respectively. The rocking curves on the $Gd_2Zr_2O_7$ (004) and Gd_2O_3 (002) reflections show a mosaic spread along the c-axis of about 6° and 7.8° for $Gd_2Zr_2O_7$ and Gd_2O_3 grains, respectively. Compared to the Ni-W substrate ($FWHM_{111}$= 6.8°), the $Gd_2Zr_2O_7$ layer has an improved out-of-plane texture. On the other hand, the out-of-plane texture in Gd_2O_3 has been degraded. The in-plane texture in Figure 7 reveals a stacking of the Gd_2O_3 (111) crystal planes on the $Gd_2Zr_2O_7$ (222) crystal planes in the (*a*,*b*) plane of the substrate. The grain mosaic spreads in the (*a*,*b*) plane were 8.4° and 9.3° for $Gd_2Zr_2O_7$ and Gd_2O_3 layer, respectively. These values indicate a degradation of the texture compared to the Ni-W substrate (phi-scan, $FWHM_{111}$= 6.5°). Larger grain dispersion was observed for the Gd_2O_3 cap layer. In addition, we noticed that increasing the Gd_2O_3 cap layer thickness did not improve significantly the in-plane texture of Gd_2O_3.

IV. Conclusion

We obtained crystalline $Gd_2Zr_2O_7$ films with high-quality surface morphology by optimizing the ethanol concentration in the electrodeposition solution mixture. After annealing in Ar:H_2 gas mixture, crystalline $Gd_2Zr_2O_7$ films were obtained with a major orientation along <001> direction. The electrodeposited Gd_2O_3/ $Gd_2Zr_2O_7$ bilayer annealed at 1100 °C for 5 h in an Ar:0.5%H_2 gas mixture yielded the best morphology and texture. Also, the Gd_2O_3/$Gd_2Zr_2O_7$ bilayer buffer architecture with a cap layer of about 20–30-nm-thick Gd_2O_3 was the best template.

Acknowledgment

We thank Bobby To of the National Renewable Energy Laboratory for SEM analysis. We are also grateful to M. Paranthaman of Oak Ridge National Laboratory for providing Ni-W tapes.

References

[1] A. Goyal, D.P. Norton, J. D. Budai, M. Paranthaman, E. D. Specht, D. M. Kroeger, D. K. Christen, Q. He, B. Saffian, F. A. List, D. F. Lee, P. M. Martin, C. E. Klabunde, E. Hartfield and V. K. Sikka, "High critical current density superconducting tapes by epitaxial deposition of YBa2Cu3Ox thick films on biaxially textured metals", *Appl. Phys. Lett.*, vol. 69, pp. 1795-, 1996.

[2] Y. Iijima, N. Tanabe, O. Kohno, and Y. Ikeno, "In-plane aligned $YBa_2Cu_3O_{7-x}$ thin films deposited on polycrystalline metallic substrates", *Appl. Phys. Lett.*, vol. 60, pp. 769-771, 1992.

[3] S. R. Foltyn, P. N. Arendt, P. C. Dowden, R. F. DePaula, J. R. Groves, J. Y. Coulter, Q. X. Jia, M. P. Maley, and D. E. Peterson, "High-T coated conductors: performance of meter-long YBCO/IBAD flexible tapes", *IEEE Trans. Appl. Supercond.*, vol. 9, pp. 1519–1522, 1999.

[4] T. Watanabe, Y. Shiohara, and T. Izumi, "Progress and Future Prospects of Research and Development on Coated Conductors in Japan", *IEEE Trans. Appl. Supercond.*, vol. 13, no. 2, pp.2445-2451, June 2003.

[5] R. Bhattacharya and S. Phok, "Electrodeposited $Gd_2Zr_2O_7$ and Gd_2O_3 Buffer Layers for $YBa_2Cu_3O_{7-\delta}$ Superconductors", *J. Electron. Mater.*, vol. 36 no. 10, pp. 1275-1278, 2007.

[6] R. Chaim, I. Silberman and L. Gal-Or, "Electrolytic ZrO_2 Coatings: II. Microstructural Aspects", *J. Electrochem. Soc.*, vol. 138 no 7, pp. 1942-1946, 1991.

[7] R. Chaim, I. Zhitomirsky, L. Gal-Or, "Electrochemical Al_2O_3-ZrO_2 composite coatings on non-oxide ceramic substrates", *J. Mater. Sci.*, vol. 32, pp. 389-400, 1997.

[8] X. Pang and I. Zhitomirsky, "Fabrication of Composite films containing Zirconia and Cationic Polyelectrolytes", *Langmuir*, vol. 20, pp. 2921-2927, 2004.

[9] I. Valov, D. Stoychev, Ts. Marinova, "Study of the kinetics of processes during electrochemical deposition of zirconia form nonaqueous electrolytes", *Electrochemica Acta.*, vol. 47, pp. 4419-4431, 2002.

[10] S. Phok and R. Bhattacharya, "Effect of samarium doping on electrodeposited CeO_2 thin film", *Phys. Stat. Sol. (a)*, vol 203 no 15, pp 3734-3742, 2006.

[11] W. Zhao, A. Norman, S. Phok and R. Bhattacharya, "Transmission electron microscope study on electrodeposited Gd2O3 and Gd2Zr2O7 buffer layers for YBa2Cu3O7-d superconductors", *Physica C*, vol 468, pp. 1092-1096, 2008.